Supporting Information

Synergistic Effects of Ternary PdO-CeO_2-OMS-2 Catalyst Afford High Catalytic Performance and Stability in the Reduction of NO with CO

Song Guo[†,#], Guomei Zhang[‡,#], Zhong-Kang Han[Δ,#], Shaoyang Zhang[†,‡], Debalaya Sarker[Δ], Wen Wu Xu[δ,*], Xiaoli Pan[†], Gao Li[†,*], and Alfons Baiker[$,*]

[†]State Key Laboratory of Catalysis, Dalian Institute of Chemical Physics, Chinese Academy of Sciences, Dalian 116023, China

[‡]School of Chemistry and Chemical Engineering, Shanxi University, Taiyuan 030006, China

[Δ]Center for Energy Science and Technology, Skolkovo Institute of Science and Technology, Skolkovo Innovation Center, Moscow, 143026, Russia

[δ]Department of Physics, School of Physical Science and Technology, Ningbo University, Ningbo, 315211, China

[$]Department of Chemistry and Applied Biosciences, Institute for Chemical and Bioengineering, ETH Zurich, Hönggerberg, HCl, CH-8093 Zurich, Switzerland

[#] S.G., Z.-K. H. and G.Z. contributed equally.

E-mail: gaoli@dicp.ac.cn (G.L.); xuwenwu@nbu.edu.cn (W.X.); alfons.baiker@chem.ethz.ch (A.B.)

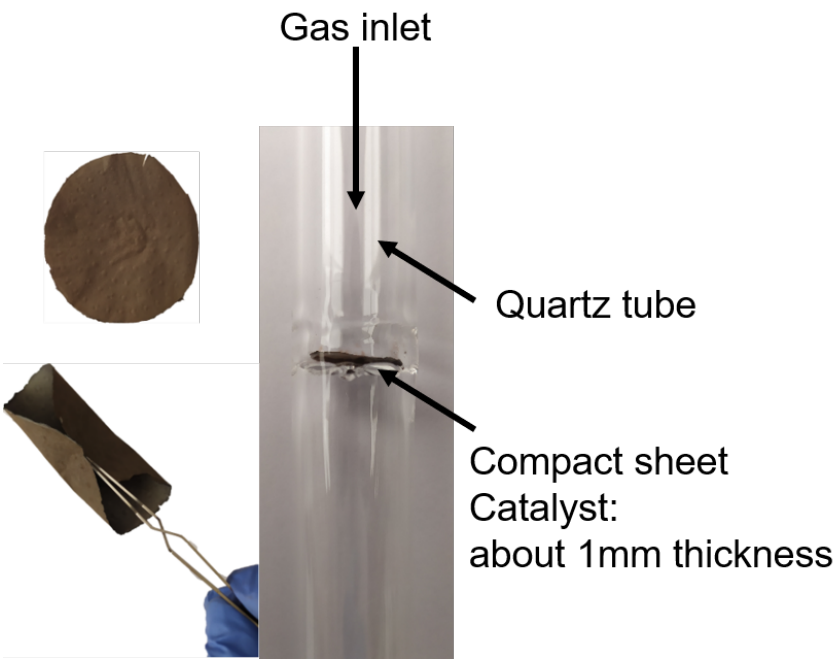

Figure S1. Flexible sheet of the PdO-CeO_2-OMS-2 composite and its arrangement in the reactor tube. The catalyst is packed as a layer of ~1 mm thickness, which is comprised of several flexible sheets.

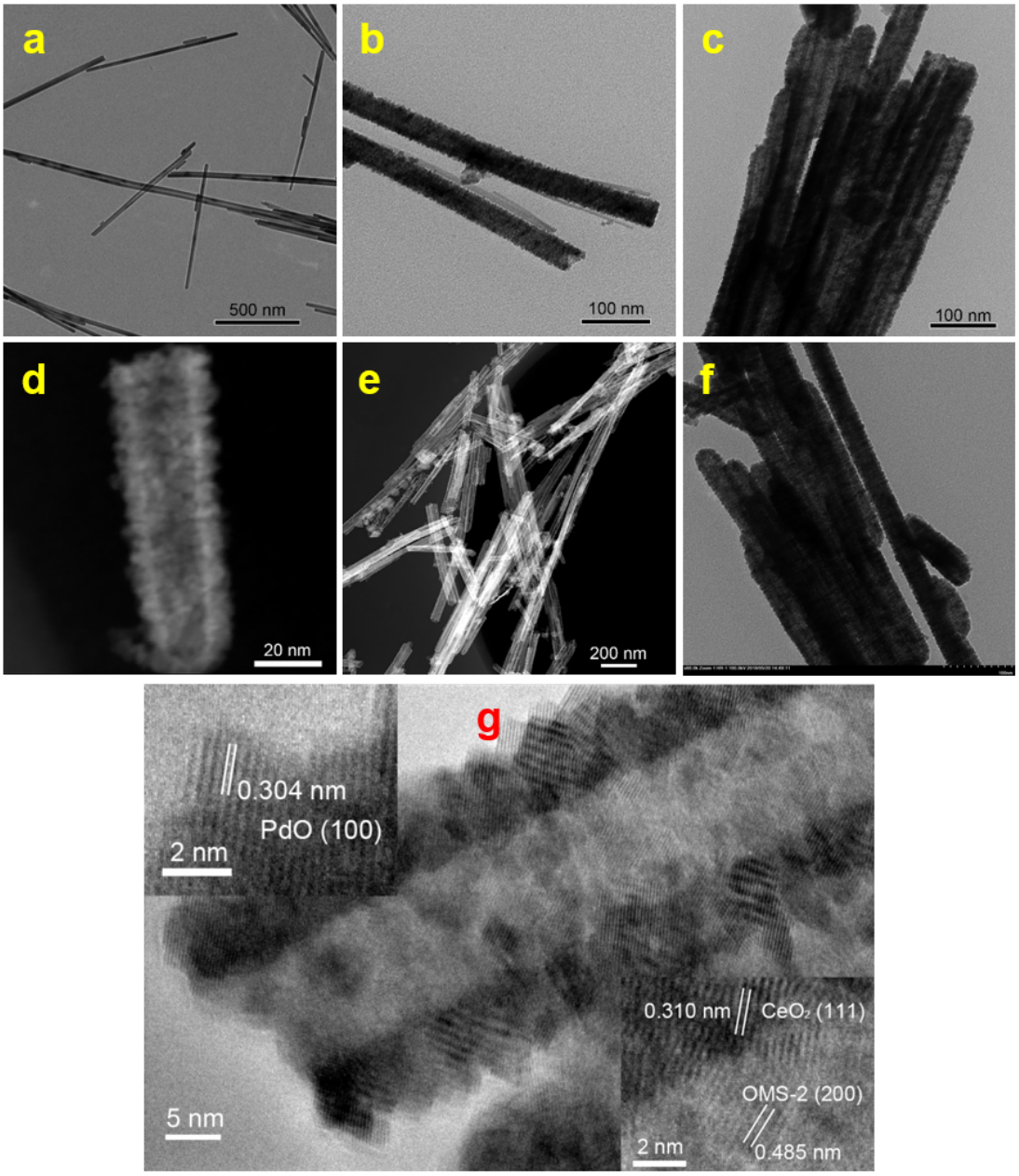

Figure S2. The representative bright field TEM images of (a) OMS-2, (b) CeO_2-OMS and (c) PdO-CeO_2-OMS samples. (d,e) STEM micrographs of PdO-CeO_2-OMS sample. The nanowire-like OMS-2 show a length varying between 500 nm to 2 μm and a width of ~20 nm. (f) The TEM image of the used PdO-CeO_2-OMS catalyst. (g) The HRTEM image of PdO-CeO_2-OMS sample.

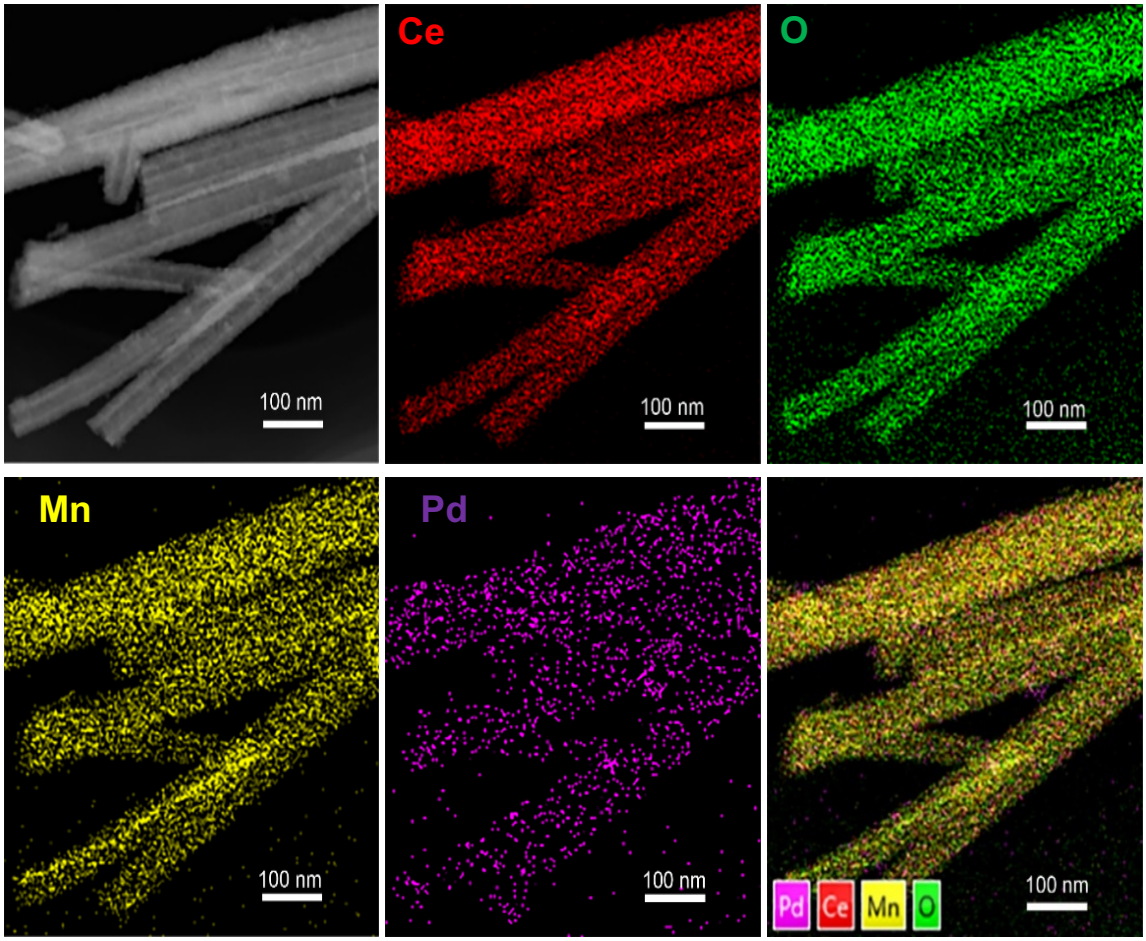

Figure S3. STEM micrograph and the corresponding Pd, Ce, Mn and O elemental mapping of PdO-CeO_2-OMS sample.

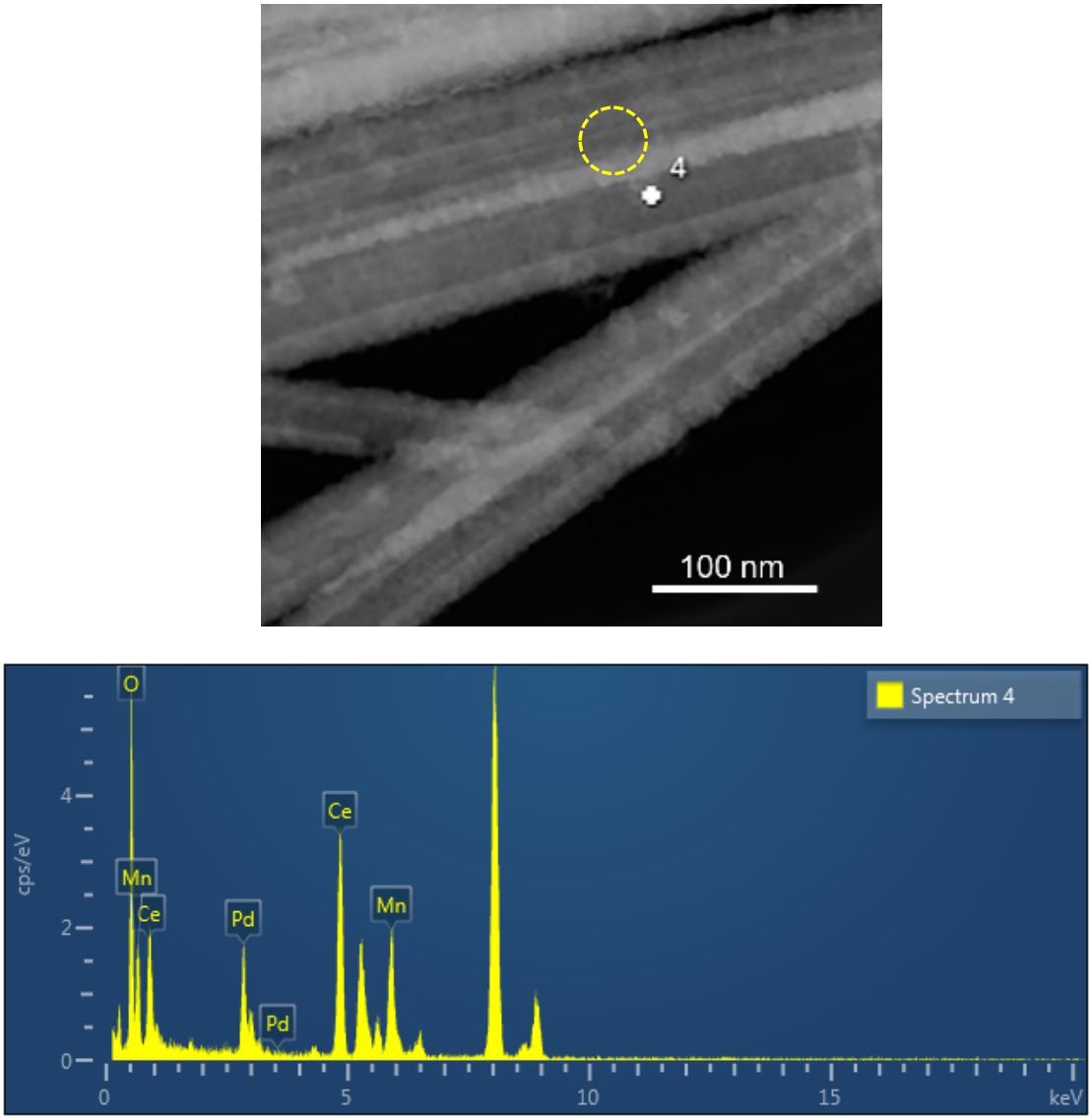

Figure S4. STEM of PdO-CeO_2-OMS catalyst and EDX of area 4.

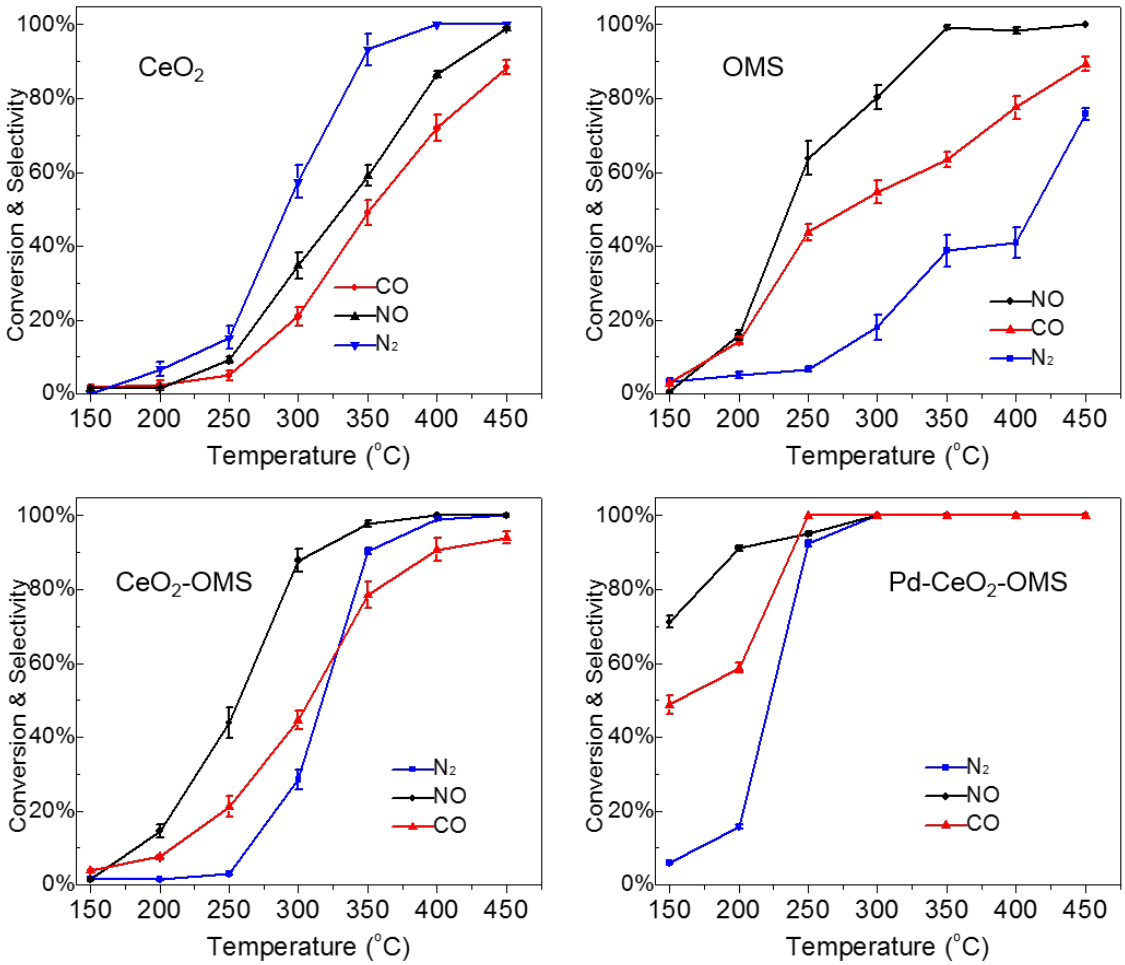

Figure S5. Conversion of CO and NO and selectivity to N_2 over the CeO_2, OMS-2, CeO_2-OMS, and PdO-CeO_2-OMS catalysts. Note that the NO conversion is higher than corresponding CO conversion. Reaction conditions: 100 mg catalysts, GHSV = 30,000 h^{-1}, 1 vol% NO and 1 vol% CO in argon balance.

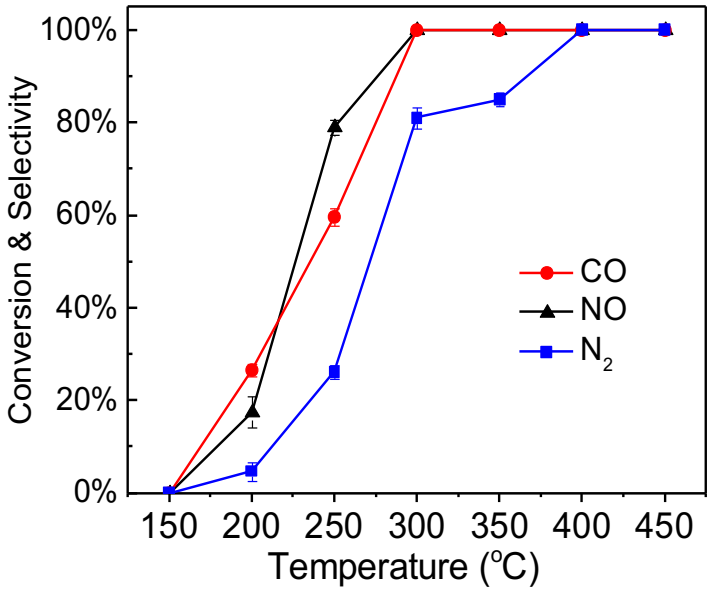

Figure S6. Catalytic performance of PdO-OMS-2 catalysts.

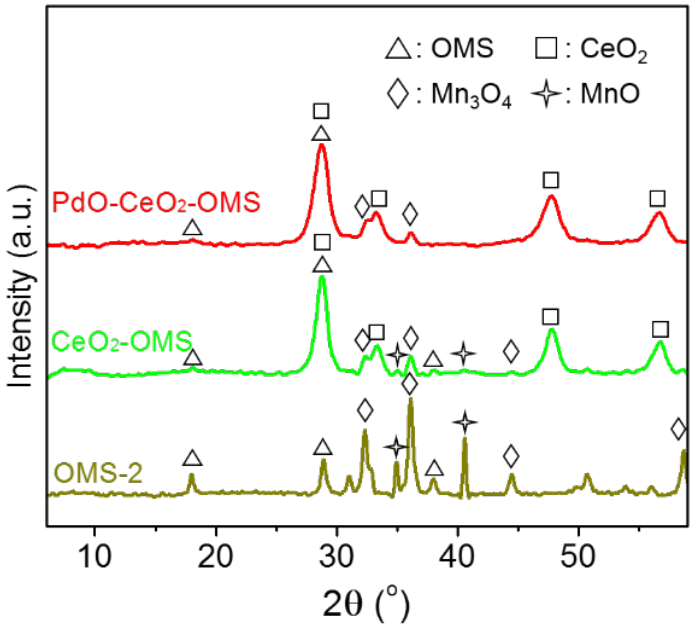

Figure S7. XRD patterns of used OMS-2, CeO_2-OMS and PdO-CeO_2-OMS-2 catalysts after the NO reduction tests.

XRD peaks of the OMS-2 are weakened after the NO-SCR reaction with CO (Figure S7) and two new diffraction peaks appeared at 36.0° and 40.6°, which belong to crystalline phase of Mn_3O_4 (JCPDS 18-0803) and MnO (JCPDS 07-0230), respectively. It indicates that the oxidation state of manganese is reduced from high state to low state during the NO reduction when using the plain OMS-2 as catalyst. For the CeO_2-OMS catalyst, only a very weak new diffraction peak appears at 36.0°, indicating that a minor part of OMS-2 composite was reduced to Mn_3O_4 species after the NO-SCR reactions. Notably, no new diffraction peak is found in the PdO-CeO_2-OMS after the NO reduction, unraveling that PdO largely impedes the reduction of OMS-2 during the NO reduction process and the catalyzed NO+CO reaction should therefore be associated with the PdO component.

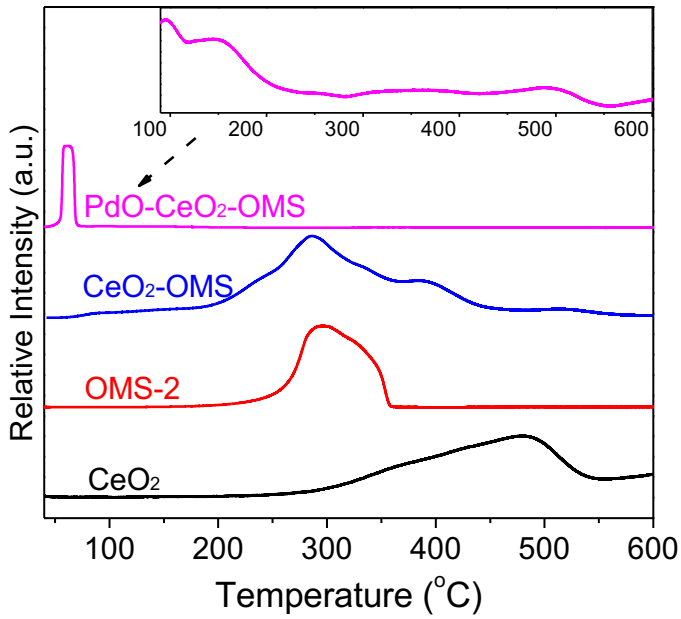

Figure S8. H_2-TPR profiles of CeO_2, OMS-2, CeO_2-OMS-2, and PdO-CeO_2-OMS-2. The inset shows the zoomed-in region beyond 100 °C for the PdO-CeO_2-OMS-2 catalyst.

The redox properties of the catalysts are closely related to the activity in CO+NO reaction. Figure S8 displays the H_2-TPR profiles of CeO_2, OMS-2, CeO_2-OMS components, and the PdO-CeO_2-OMS catalysts. CeO_2 shows a broad reduction peak starting from 290 °C to 530 °C, representing the removal of surface oxygen of CeO_2. OMS-2 gives rise to a strong peak around 300 °C with a shoulder around 325 °C, which is due to the reduction of MnO_2/Mn_2O_3 to Mn_3O_4/MnO. A series of peaks between 200 °C and 420 °C are observed for CeO_2-OMS; the peaks ~300 °C and 400 °C correspond to the OMS-2 reduction and the reduction of surface Ce^{4+} to Ce^{3+}, respectively. It is worthy to note that the reduction process of OMS-2 is accompanied by the reduction of surface CeO_2 in the range of 330-420 °C, resulting in lower reduction temperature for surface CeO_2. It suggests some interaction between ceria and MnO_x. PdO-CeO_2-OMS-2 shows a sharp reduction peak at 60 °C, which is attributed to reduction of the PdO species at interface to metallic Pd^0. The other reductive peaks at 100 °C and 150 °C are assigned to the reduction of [O] on the surface of CeO_2-OMS,[1] implying that PdO nanoparticles can promote hydrogen adsorption and electron transfer to the oxide surfaces thereby enhancing the catalytic performance in the NO reduction.[2,3]

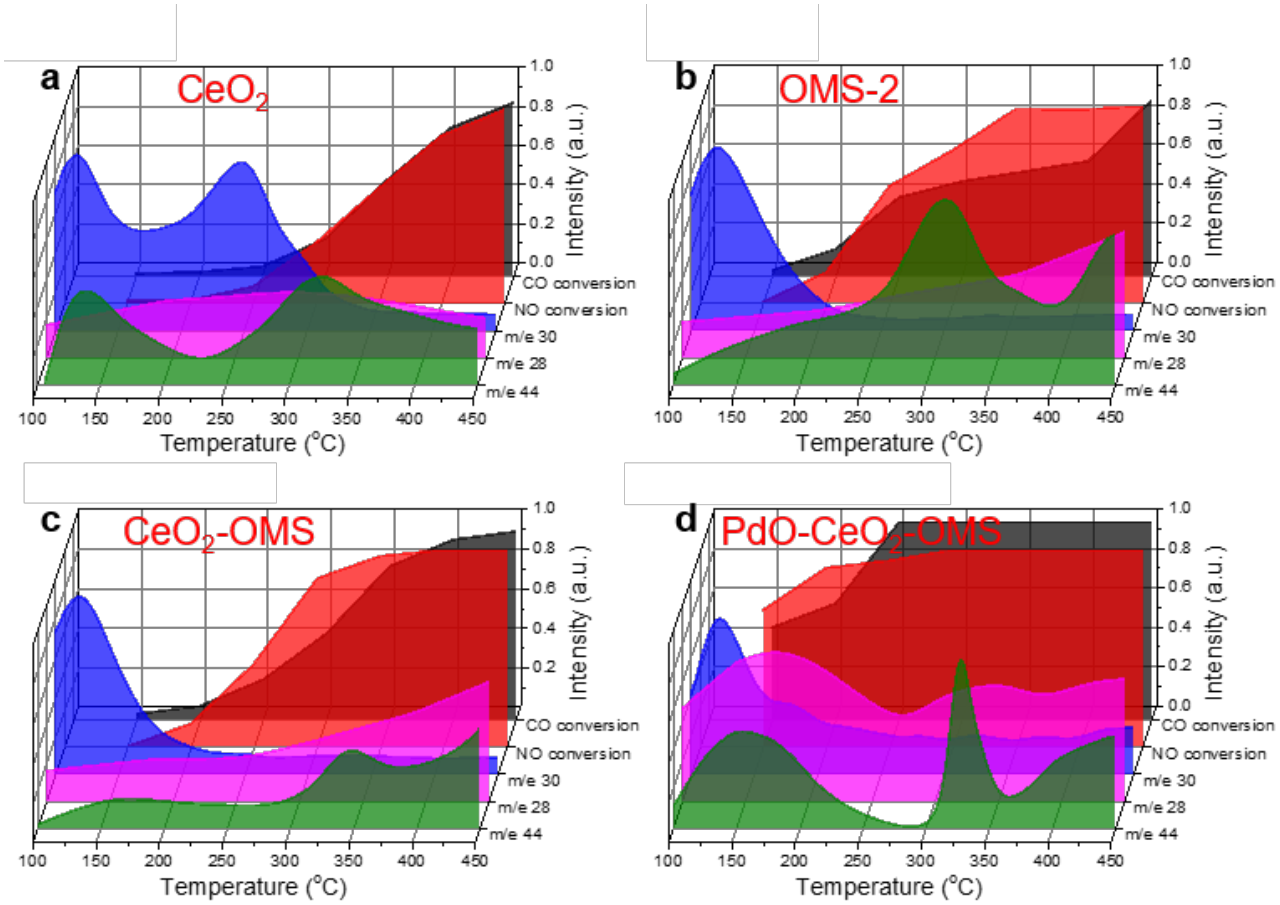

Figure S9. The normalized contrast profiles of (CO+NO)-TPD and conversion of CO and NO on (a) CeO_2, (b) OMS-2, (c) CeO_2-OMS-2 components, and (d) PdO-CeO_2-OMS-2 catalyst. *m/e* =28, 30 and 44 are assigned to signals of (CO or N_2), NO and (CO_2 and N_2O), respectively. The MS monitoring was supported by GC analyses.

In the CO+NO-TPD experiment, 50 mg catalyst was loaded into a U-shape quartz reactor and purged with N_2 at 300 °C for 2 h to remove adsorbed carbonates and hydrates. Then the system was cooled to room temperature and the N_2 flow of 10 mL min^{-1} was switched to 1 vol% NO and 1 vol% CO (balance argon) mixed gas flow for 30 mins. After this exposure, the flow was changed to argon with same flowrate and the temperature was ramped from 100 °C to 450 °C at a rate of 10 °C/min. Desorbing gases were monitored by MS and GC analyses.

We correlated the relationship of the normalized (CO+NO)-TPD profiles and conversion curves of CO and NO. In the normalized (CO+NO)-TPD profiles, the signal peaks of *m/e* 28, 30 and 44 represent CO and N_2, desorption of NO, and N_2O and CO_2 products, respectively. The NO

desorption occurred at ~115 ºC for OMS-2 and CeO_2-OMS. While, for CeO_2 and PdO-CeO_2-OMS it appeared at ~115 ºC and >200 ºC, which indicates that the NO molecules were strongly bound to the CeO_2 and PdO-CeO_2-OMS. As concerns the signal of *m/e* 28, CeO_2, OMS-2, and CeO_2-OMS showed no distinct peaks up to 300 ºC, demonstrating that the adsorption of CO on these samples is relatively weak. For comparison, the PdO-CeO_2-OMS sample showed a peak at 150 ºC, unraveling that CO was selectively adsorbed and activated on the surface of the PdO particles. These results are in line with the XPS analyses of the used PdO-CeO_2-OMS catalysts (Figure 5). Note that the peak of *m/e* 28 at 150 ºC here is assigned to CO, as confirmed by GC and also supported by the fact that the selectivity to N_2 is close to zero in the NO reduction at 150 ºC (Figure 4c). The desorption trend of the mass peak *m/e* 28 (the yield of N_2O and CO_2) is consistent with the observed conversion of CO and NO.

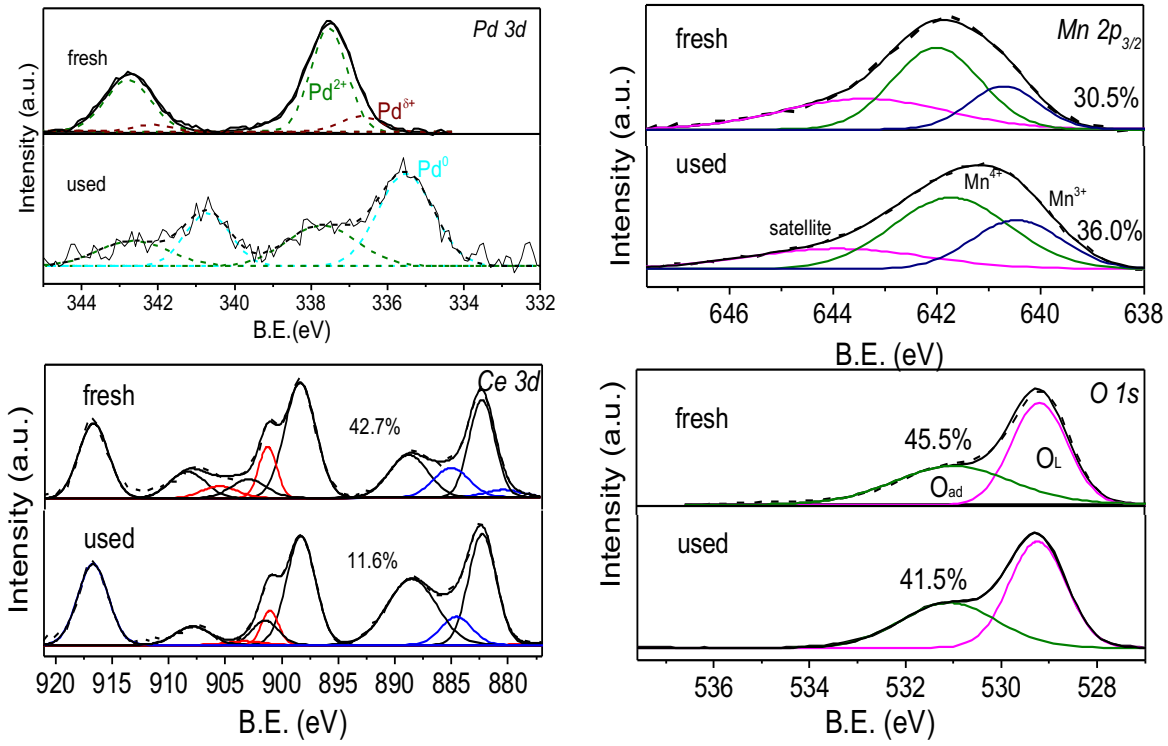

Figure S10. Pd 3d, Mn $2p_{3/2}$, Ce 3d and O 1s XPS spectra of fresh and used PdO-CeO_2-OMS-2 catalyst. The red and blue peaks are the B.E. peaks of Ce^{3+} species in Ce 3d.

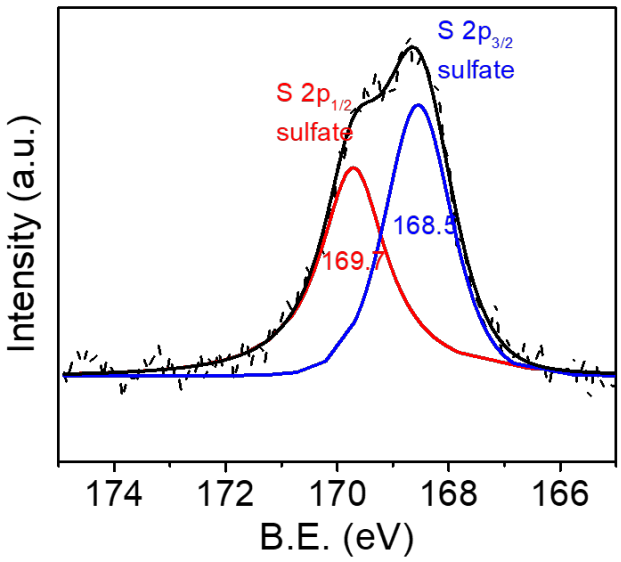

Figure S11. S2p XPS spectrum of the spent PdO-CeO_2-OMS catalyst after experiments shown in Figure 6c with a feed containing 5% H_2O and 100 ppm SO_2.

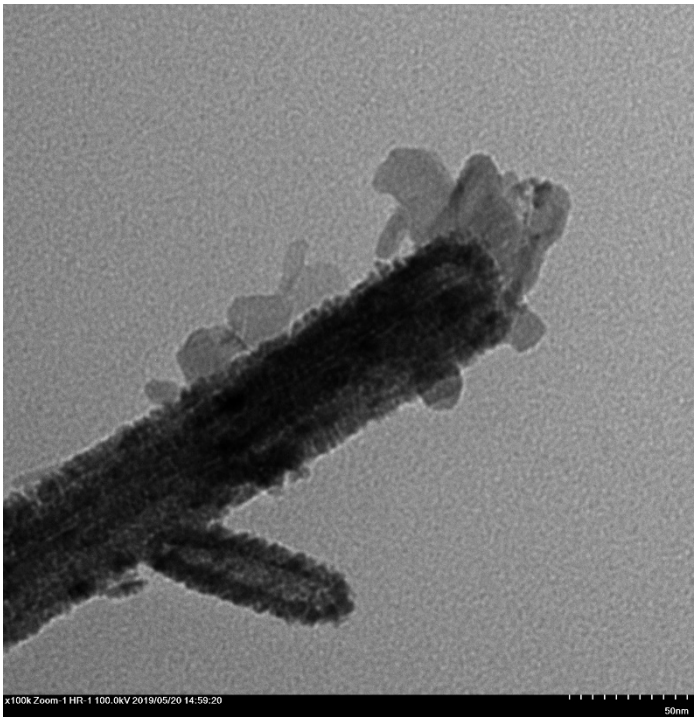

Figure S12. Typical TEM image of the spent PdO-CeO_2-OMS-2 catalyst.

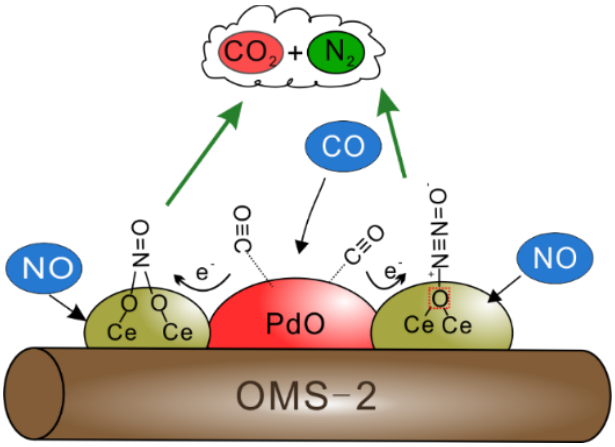

Scheme S1. Proposed mechanism for the reduction of NO with CO over the ternary PdO-CeO_2-OMS-2 catalyst.

Table S1. Summary of XPS analysis of the fresh and spent catalysts. The values in the parentheses are assigned to the spent catalysts.

	species	CeO_2	OMS-2	CeO_2-OMS	PdO-OMS	PdO-CeO_2-OMS
Mn2p	Mn^{3+}/mol%		23.3 (41.4)	31.0 (38.6)	30.9 (47.8)	30.5 (36.0)
	Mn^{4+}/mol%		76.7 (58.6)	69.0 (61.4)	69.1 (52.2)	69.5 (64.0)
	Mn^{4+}/Mn^{3+}		3.3 (1.4)	2.2 (1.6)	2.2 (1.1)	2.3 (1.8)
Ce3d	Ce^{3+}/mol%	42.3 (14.3)		36.2 (18.8)		42.7 (11.6)
	Ce^{4+}/mol%	57.7 (85.7)		63.8 (81.2)		57.3 (88.4)
	Ce^{4+}/Ce^{3+}	1.4 (6.0)		1.7 (4.3)		1.3 (**7.6**)
O1s	O_{latt}/mol%	36.4 (59.2)	78.1 (48.7)	61.2 (57.0)	65.3 (61.4)	54.5 (58.5)
	O_{ads}/mol%	25.3 (40.8)	21.9 (43.2)	38.8 (43.0)	34.7 (38.6)	45.5 (41.5)
	CO_3^{2-}/OH^-	38.3 (0)	0 (8.1)	0 (0)	0 (0)	0 (0)
	O_{ads}/O_{latt}	0.69 (0.69)	0.28 (0.88)	0.63 (0.75)	0.53 (0.63)	0.83 (**0.71**)
Pd3d	Pd^{2+}/mol%					87.8 (38.5)
	Pd^0/mol%					12.2 (61.5)
	Pd^{2+}/Pd^0					7.2 (**0.63**)

Table S2. Comparison of catalytic performances of representative catalysts for the reduction of NO with CO reported in the literature.

Catalysts	Component	Catalyst usage (mg)	NO vol. (ppm)	Gas flow (h^{-1})	100% conv. T (°C)	Durability (h)	X_{NO} & S_{N2} (%)	Reagent (ppm)	Ref.
NiO/CeO_2 (DP)	Ni, Ce	100	2,500	120,000	250	-	100&100	CO: 2500	4
NiO/CuO	Ni, Cu	125	10,000	9600	350	-	100&90	CO: 10,000	5
Fe_2O_3/CeO_2	Fe, Ce	-	800	30,000	200	-	100&90	CO: 1600	6
Fe-Co catalyst	Fe, Co	2,000	10,000	6000	300	-	100&100	CO: 20,000	7
$Au@Fe_2O_3/CeO_2$	Au, Fe, Ce	50	3000	3000	300	-	95&98	CO:3000; H_2:1000	8
$Ir-Au/Al_2O_3$	Ir, Au, Al	200	2000	6000	350	-	98&-	CO: 2000	9
Fe-Zr catalyst	Fe, Zr	1000	1000	90,000	350	-	100&100	CO: 7000	10
$Mn_3O_4@C$	Mn, C	218-872	600	60,000	290	8	90&90	NH_3: 660	11
Fe-V oxide	Fe, V	25	500	24,000	300	-	90&100	NH_3:500	12
$VO_x/CeO_2@MnO_x$	V, Ce, Mn	200	500	160,000	300	-	95&100	NH_3:500	13
MnO_x/Al_2O_3	Mn, Al	-	500	35,000	300	-	95&100	NH_3:500	14
CeO_2-TiO_2	Ce, Ti	-	500	90,000	300	-	98&95	NH_3:500	15
$Au-Ce/Al-TiO_x$	Au, Ce, Al	600	500	9,000	300	16	100&100	CO:500	16
$Ce_xSn_{1-x}O_2$	Ce, Sn	50	50,000	600	300	-	45&90	CO:100,000	17
$CuO@ZrO_2$-TiO_2	Cu, Zr, Ti	50	50,000	12,000	300	-	100&95	CO:100,000	18
$CuO/Ce_xZr_{1-x}O_2/Al_2O_3$	Cu, Ce, Zr, Al	50	50,000	12,000	300	-	100&100	CO: 100,000	19
$Pt/WO_3/CeO_2/ZrO_2$	Pt, W, Ce, Zr	500	5,000	40,000	300	-	<20&-	CO: 5,000	20
PdO-CeO_2-OMS	Pd, Ce, Mn	100	10,000	30,000	300	150	100&100	CO:10,000	This work

Table S3. Chemical elemental analysis of catalysts from ICP-OES analysis

Catalyst	Pd content	Mn content	Ce content
PdO-CeO_2-OMS-2	1.6 wt.%	15.6 wt.%	51.1 wt.%

References

(1) Zhang, X. Y.; Wei, J. J.; Yang, H. X.; Liu, X. F.; Liu, W.; Zhang, C.; Yang, Y. Z. One-Pot Synthesis of Mn-Doped CeO_2 Nanospheres for CO Oxidation. *Eur. J. Inorg. Chem.* **2013**, *2013* (25), 4443-4449.

(2) Yao, X. J.; Tang, C. J.; Ji, Z. Y.; Dai, Y.; Cao, Y.; Gao, F.; Dong, L.; Chen, Y. Investigation of the Physicochemical Properties and Catalytic Activities of $Ce_{0.67}M_{0.33}O_2$ (M = Zr^{4+}, Ti^{4+}, Sn^{4+}) Solid Solutions for No Removal by CO. *Catal. Sci. Technol.* **2013**, *3* (3), 688-698.

(3) Sun, C. Z.; Tang, Y. J.; Gao, F.; Sun, J. F.; Ma, K. L.; Tang, C. J.; Dong, L. Effects of Different Manganese Precursors as Promoters on Catalytic Performance of CuO–MnO_x/TiO_2 Catalysts for NO Removal by CO. *Phys. Chem. Chem. Phys.* **2015**, *17* (24), 15996-16006.

(4) Wang, Y.; Zhu, A.; Zhang, Y.; Au, C. T.; Yang, X.; Shi, C. Catalytic Reduction of NO by CO over NiO/CeO_2 Catalyst in Stoichiometric NO/CO and NO/CO/O_2 Reaction. *Appl. Catal. B Environ.* **2008**, *81* (1), 141-149.

(5) Copper-Nickel Catalysts from Hydrotalcite Precursors: The Performance in NO Reduction by CO. *Appl. Catal. B Environ.* **2018**, *237*, 327-338.

(6) Cheng, X.; Zhang, X.; Su, D.; Wang, Z.; Chang, J.; Ma, C. NO Reduction by CO over Copper Catalyst Supported on Mixed CeO_2 and Fe_2O_3: Catalyst Design and Activity Test. *Appl. Catal. B: Environ.* **2018**, *239*, 485-501.

(7) Wang, L.; Cheng, X.; Wang, Z.; Ma, C.; Qin, Y. Investigation on Fe-Co Binary Metal Oxides Supported on Activated Semi-Coke for No Reduction by CO. *Appl. Catal. B Environ.* **2017**, *201*, 636-651.

(8) Ilieva, L.; Pantaleo, G.; Velinov, N.; Tabakova, T.; Petrova, P.; Ivanov, I.; Avdeev, G.; Paneva, D.; Venezia, A. M. NO Reduction by CO over Gold Catalysts Supported on Fe-Loaded Ceria. *Appl. Catal. B Environ.* **2015**, *174-175*, 176-184.

(9) Song, Y.-J.; Jesús, Y. M. L.-D.; Fanson, P. T.; Williams, C. T. Kinetic Evaluation of Direct No Decomposition and NO–CO Reaction over Dendrimer-Derived Bimetallic Ir–Au/Al_2O_3 Catalysts. *Appl. Catal. B Environ.* **2014**, *154-155*, 62-72.

(10) France, L. J.; Li, W.; Zhang, Y.; Mu, W.; Chen, Z.; Shi, J.; Zeng, Q.; Li, X. A Superior Fe-Zr Mixed Oxide Catalyst for the Simultaneous Reduction of NO and SO_2 with CO. *Appl. Catal. B: Environ.* **2020**, *269*, 118822.

(11) Liu, Z.; Wang, M.; Liu, S.; Chen, Z.; Yang, L.; Sun, K.; Chen, Y.; Zeng, L.; Wang, W.; Zhao, J.; Sun, G.; Liu, B.; Pan, Y.; Liu, Y.; Liu, C. Design of Assembled Composite of Mn_3O_4@Graphitic Carbon Porous Nano-Dandelions: A Catalyst for Low–Temperature Selective Catalytic Reduction of NO_x with Remarkable SO_2 Resistance. *Appl. Catal. B: Environ.* **2020**, *269*, 118731.

(12) Li, Y.; Liu, W.; Yan, R.; Liang, J.; Dong, T.; Mi, Y.; Wu, P.; Wang, Z.; Peng, H.; An, T. Hierarchical Three-Dimensionally Ordered Macroporous Fe-V Binary Metal Oxide Catalyst for Low Temperature

Selective Catalytic Reduction of NO_x from Marine Diesel Engine Exhaust. *Appl. Catal. B: Environ.* **2020**, *268*, 118455.

(13) Wu, X.; Yu, X.; Huang, Z.; Shen, H.; Jing, G. Mnox-Decorated VO_x/CeO_2 Catalysts with Preferentially Exposed {110} Facets for Selective Catalytic Reduction of Nox by NH_3. *Appl. Catal. B: Environ.* **2020**, *268*, 118419.

(14) Yang, G.; Zhao, H.; Luo, X.; Shi, K.; Zhao, H.; Wang, W.; Chen, Q.; Fan, H.; Wu, T. Promotion Effect and Mechanism of the Addition of MO on the Enhanced Low Temperature Scr of NOx by NH_3 over MnO_x/Γ-Al_2O_3 Catalysts. *Appl. Catal. B: Environ.* **2019**, *245*, 743-752.

(15) Liu, H.; Fan, Z.; Sun, C.; Yu, S.; Feng, S.; Chen, W.; Chen, D.; Tang, C.; Gao, F.; Dong, L. Improved Activity and Significant SO_2 Tolerance of Samarium Modified CeO_2-TiO_2 Catalyst for NO Selective Catalytic Reduction with NH_3. *Appl. Catal. B Environ.* **2019**, *244*, 671-683.

(16) Striking Activity Enhancement of Gold Supported on Al-Ti Mixed Oxide by Promotion with Ceria in the Reduction of NO with CO. *Appl. Catal. B: Environ.* **2017**, *209*, 62-68.

(17) Yao, X.; Xiong, Y.; Zou, W.; Zhang, L.; Wu, S.; Dong, X.; Gao, F.; Deng, Y.; Tang, C.; Chen, Z.; Dong, L.; Chen, Y. Correlation between the Physicochemical Properties and Catalytic Performances of $Ce_xSn_{1-x}O_2$ Mixed Oxides for NO Reduction by CO. *Appl. Catal. B: Environ.* **2014**, *144*, 152-165.

(18) Sun, C.; Zhu, J.; Lv, Y.; Qi, L.; Liu, B.; Gao, F.; Sun, K.; Dong, L.; Chen, Y. Dispersion, Reduction and Catalytic Performance of CuO Supported on ZrO_2-Doped TiO_2 for NO Removal by CO. *Appl. Catal. B: Environ.* **2011**, *103* (1), 206-220.

(19) Yu, Q.; Liu, L.; Dong, L.; Li, D.; Liu, B.; Gao, F.; Sun, K.; Dong, L.; Chen, Y. Effects of Ce/Zr Ratio on the Reducibility, Adsorption and Catalytic Activity of $CuO/CexZr_{1-x}O_2/\Gamma$-$Al_2O_3$ Catalysts for NO Reduction by CO. *Appl. Catal. B: Environ.* **2010**, *96* (3), 350-360.

(20) Zhu, H.-o.; Kim, J.-R.; Ihm, S.-K. Characteristics of $Pt/WO_3/CeO_2/ZrO_2$ Catalysts for Catalytic Reduction of NO by CO. *Appl. Catal. B: Environ.* **2009**, *86* (1), 87-92.